Letter

Josephson current signature of Floquet Majorana and topological accidental zero modes in altermagnet heterostructures

Amartya Pal [1,2] Debashish Mondal [1,2] Tanay Nag [3,*] and Arijit Saha [1,2,†]

[1] *Institute of Physics, Sachivalaya Marg, Bhubaneswar 751005, India*

[2] *Homi Bhabha National Institute, Training School Complex, Anushakti Nagar, Mumbai 400094, India*

[3] *Department of Physics, BITS Pilani-Hydrabad Campus, Telangana 500078, India*

(Received 13 May 2025; revised 5 November 2025; accepted 7 November 2025; published 24 November 2025)

We theoretically investigate the generation and Josephson current signatures of Floquet Majorana end modes (FMEMs) in a periodically driven altermagnet (AM) heterostructure. Considering a one-dimensional (1D) Rashba nanowire (RNW) proximitized to a regular s-wave superconductor (SC) and a d-wave AM, we generate both 0- and π-FMEMs by driving the nontopological phase of the static system. Interestingly, the static counterpart hosts both topological Majorana zero modes (MZMs) and inquisitive nontopological accidental zero modes (AZMs) not originating from any metal-SC interface but rather intrinsic to the bulk of the isolated system. The periodic drive can gap out the static AZMs and generate robust π-FMEMs, termed as topological AZMs. We topologically characterize the emergent FMEMs via dynamical winding numbers exploiting chiral symmetry of the system. Moreover, we consider a periodically driven Josephson junction comprising a RNW/AM-based 1D topological superconduting setup. We identify the signature of MZMs and FMEMs utilizing the 4π-periodic Josephson effect, distinguishing them from trivial AZMs exhibiting 2π periodicity, in both static and driven platforms. This Josephson current signal due to Majorana modes survives even in the presence of finite disorder. Our Letter establishes a route to realize and identify FMEMs in AM-based platforms through Floquet engineering and Josephson current response.

DOI: 10.1103/prnx-47mk

Introduction. The hunt for realizing topological superconductors (TSCs) hosting Majorana zero modes (MZMs) has driven intense research interest for decades. The non-Abelian braiding statistics of MZMs enable them as a promising candidate for decoherence-free topological quantum computation [1–16]. MZMs, the charge-neutral zero-energy quasiparticle excitations in TSCs, were theoretically proposed in one-dimensional (1D) spinless p-wave superconductors (SCs) by Kitaev [1], and later proposed to be engineered in Rashba nanowires (RNWs) with strong spin-orbit coupling (SOC), placed in close proximity to a s-wave SC under an external Zeeman field [2–5]. Owing to resonant Andreev reflection, a pair of MZMs exhibits a zero bias conductance peak (ZBCP) at zero temperature, quantized at $2e^2/h$ [17–25]. Experimental detection of such ZBCP via differential conductance (dI/dV) measurement is often considered as an indirect signature of MZMs [22–25]. However, various alternative phenomena, e.g., Andreev bound states [26–28], Kondo resonance [29,30], and disorder [31], can also produce a ZBCP, leading to dispute in MZMs detection. In sharp contrast, the 4π-periodic Josephson effect serves as a promising signature of MZMs [3–6,32–39] and cannot be replicated in other physical systems. When two weakly coupled TSCs with a superconducting phase difference, ϕ, form a Josephson junction (JJ), the Josephson current (JC) exhibits 4π periodicity due to tunneling of MZMs across the junction unlike the usual 2π periodicity in conventional JJs, where only Cooper pairs contribute [3,6]. This 4π periodicity originates from the global conservation of ground state fermionic parity [3,32].

In current literature, altermagnets (AMs) are proposed to be a new class of antiferromagnets with even parity collinear-compensated magnetic order where two opposite spin sublattices are connected through rotation rather than only translation, e.g., C_4 rotation in d-wave AMs [40–46]. Interestingly, regardless of the net zero magnetization, AMs break time-reversal symmetry and host unique spin-split band structures due to anisotropic momentum-dependent exchange interactions as observed in RuO_2, MnTe, CrSb, MnF_2, etc. [40–43,47,48]. Very recently, generation of MZMs and nontopological accidental zero modes (AZMs) using AMs has been proposed by replacing the external Zeeman field in 1D RNW systems [18,49–59]. The net zero magnetization is advantageous for sustaining proximity induced superconductivity. In recent times, various phenomena in AM-based JJs are also investigated in the literature [60–63]. However, identifying MZMs and AZMs in the JJ setup based on AM-SC heterostructure remains to be addressed.

On the other hand, one promising approach to engineer Majorana modes is via Floquet engineering where a time periodic drive generates topologically nontrivial states in quantum materials [64–83]. Interestingly, an external time-periodic drive can generate topologically protected Majorana modes both at zero and finite quasienergy, namely 0- and π- Floquet Majorana end modes (FMEMs) respectively, even starting

*Contact author: tanay.nag@hyderabad.bits-pilani.ac.in

†Contact author: arijit@iopb.res.in

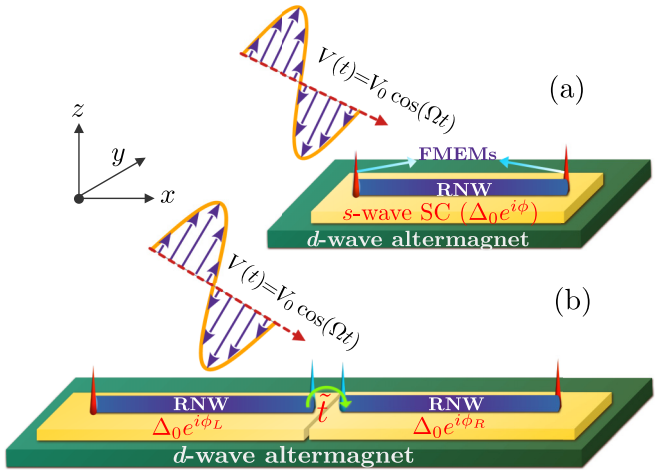

FIG. 1. Schematic illustration of our AM-SC heterostructure. (a) A 1D RNW (blue) is placed in close proximity to a s-wave SC (yellow) and a d-wave AM (green) in presence of an external sinusoidal Floquet drive, $V(t)$. This setup hosts FMEMs localized at the ends of the RNW (red spikes). Panel (b) depicts the JJ setup composed of two weakly coupled TSCs [as shown in panel (a)], with coupling strength $\tilde{t}$ and superconducting phase bias, $\phi = (\phi_L - \phi_R)$. This setup is periodically driven by $V(t)$.

from the nontopological phase of a system. Generation of FMEMs and their dI/dV signature by periodically driving the static TSCs is investigated in the literature [84–94]. However, the effect of the external time periodic drive in AM-SC heterostructures remains unexplored. Furthermore, the signature of FMEMs and the dynamical version of AZMs via JC response still remain interesting avenues to address. Very recently, the JC response of FMEMs has been investigated for driven JJs of 1D p-wave Kitaev chains [95].

Given the above background, in this Letter, we pose the following key questions.

(i) Is it possible to transform the static trivial AZMs to topological accidental zero modes (TAZMs) with drive?

(ii) In the static case, can MZMs be distinguished from AZMs via JC signatures?

(iii) In the driven scenario, can TAZMs be identified utilizing the energy resolved Floquet JC formalism?

To answer these intriguing questions, we consider a heterostructure consisting of a 1D RNW proximitized to a d-wave AM and s-wave SC, and drive the system with a sinusoidal time-periodic gate voltage, $V(t)$, as illustrated in Fig. 1(a). First, driving the nontopological phase of the static model, we generate both 0- and π-FMEMs and topologically characterize the emergent Floquet TSC phase using dynamical winding numbers (DWNs). Importantly considering the model parameters that support AZMs in the static system [18], we demonstrate AZMs can be fully gapped out by suitably tuning the driving frequency and amplitude. Interestingly, this procedure not only eliminates AZMs but also generates robust TAZMs manifested as π-FMEMs. Afterwards, we construct a JJ as shown in Fig. 1(b) formed by two weakly coupled TSCs with a superconducting phase bias, ϕ. For the undriven JJ, the junction localized MZMs display the unusual 4π-periodic Josephson effect, manifested as discontinuity in JC at $\phi = \pi$ owing to its topological origin. In contrast, AZMs do not show such feature and exhibit 2π periodicity in JC signifying their nontopological nature. Interestingly, the TAZMs, obtained by driving the static AZMs, exhibit the 4π-periodic Josephson effect indicating the topological character of them induced by the external drive.

Static model Hamiltonian. We begin with the static Bogoliubov–de Gennes (BdG) Hamiltonian in real space representing the 1D RNW of length N_x hosting proximity induced s-wave superconductivity and the magnetic order of a d-wave AM as shown in Fig. 1(a) [18,49]:

$$\mathcal{H}_0 = \sum_{x,x'=1}^{N_x} \Psi_x^\dagger H_{x,x'} \Psi_x' + \text{H.c.},$$

where

$$H_{x,x'} = \tfrac{1}{2}[t\,\pi_z\sigma_0 - i\lambda_R\,\pi_z\sigma_y + J_A\,\pi_0\sigma_z]\delta_{x',x+1} \times [-\mu\,\pi_z\sigma_0 + \Delta_0 e^{i\phi}\,\pi_x\sigma_0]\delta_{x',x}. \quad (1)$$

Here, the BdG basis is chosen as $\Psi_x = (c_{x\uparrow}, c_{x\downarrow}, -c_{x\downarrow}^\dagger, c_{x\uparrow}^\dagger)^T$, where $c_{xs}(c_{xs}^\dagger)$ denotes the annihilation (creation) operator of an electron at site x with spin $s = (\uparrow, \downarrow)$. The model parameters t, μ, λ_R, and J_A represent the strength of hopping amplitude, chemical potential, Rashba SOC, and d-wave altermagnetic strength, respectively, while Δ_0 and ϕ correspond to the proximity induced superconducting gap and phase. The Pauli matrices $\boldsymbol{\pi}(\boldsymbol{\sigma})$ act on the particle-hole (spin) subspace. The static model in Eq. (1) belongs to the BDI topological class [96] as chiral ($\mathcal{S}$), charge-conjugation ($\mathcal{C}$), and pseudo-time-reversal symmetry ($\mathcal{T}'$) are preserved [7,18] with $\mathcal{S} = \pi_y\sigma_y$, $\mathcal{C} = \pi_y\sigma_y\mathcal{K}$, and $\mathcal{T}' = \mathcal{K}$ where $\mathcal{K}$ is the complex conjugation operator. The static Hamiltonian hosts MZMs for $\sqrt{(t-\mu)^2 + \Delta_0^2} \leqslant |J_A| \leqslant \sqrt{(t+\mu)^2 + \Delta_0^2}$ and AZMs for $\mu = 0, |J_A| \geqslant t$ [18]. For the rest of the paper, we set $t = 1$, $\Delta_0 = 0.3t$, and $\lambda_R = 0.5t$ for simplicity while other model parameter values are explicitly mentioned. In Fig. 1(a) we choose $\phi = 0$ while allowing ϕ to take a nonzero value in the JJ setup [see Fig. 1(b)].

Generation and topological characterization of FMEMs. We periodically drive the static Hamiltonian to realize FMEMs using a time-periodic sinusoidal modulation to the chemical potential in Eq. (1) as

$$\mu(t) = \mu + V_0\cos(\Omega t).$$

Therefore, the time-periodic part of the driven system is then expressed in the BdG basis as

$$V(t) = \sum_{x=1}^{N_x} \Psi_x^\dagger [V_0\cos(\Omega t)\pi_z\sigma_0]\Psi_x, \quad (2)$$

where V_0 and $\Omega\,(= 2\pi/T)$ are the amplitude and frequency of the Floquet drive, respectively, with T being the time period of the drive. The time periodicity of $V(t)$, i.e., $V(t+T) = V(t)$, renders the full Hamiltonian $\mathcal{H}(t) = \mathcal{H}_0 + V(t)$ time periodic with period T. Utilizing the Floquet theorem, the solution of the time-dependent Hamiltonian can be expressed as $|\psi_\alpha(t)\rangle = e^{-iE_\alpha t}|\varphi_\alpha(t)\rangle$ where $\{E_\alpha\}$ and $\{|\varphi_\alpha(t)\rangle\}$ are the quasienergies and Floquet eigenstates of the system [71,72,97]. For a time span large compared to a single

time period, T, the quasienergies, $\{E_\alpha\}$, are procured in a stroboscopic fashion by diagonalizing the effective time-independent Floquet Hamiltonian, $\mathcal{H}_F$, defined as [71]

$$\exp(-i\mathcal{H}_F T) \equiv \hat{\mathrm{TO}} \exp\left[-i\int_0^T \mathcal{H}(t)dt\right], \tag{3}$$

where $\hat{\mathrm{TO}}$ corresponds to the time-ordering operator. We numerically compute the quasienergies $\{E_\alpha\}$ efficiently employing the second-order Trotter-Suzuki formalism [81,98–100]. Note that in the real-time picture E_α is restricted to be in the range $[-\Omega/2, \Omega/2]$, known as the first Floquet Brillouin zone. Following the literature, we call the Floquet modes with energy $E_\alpha = 0$ and $\Omega/2$ as 0-FMEMs and π-FMEMs, respectively [81,92,93]. For the purpose of topological characterization of 0- and π-FMEMs, we compute the DWNs, $\mathcal{W}_0$ and $\mathcal{W}_\pi$, exploiting the chiral symmetry, $\mathcal{S}$, of the system [see Supplemental Material (SM) [101] for detailed derivation] as [69,82,102]

$$\mathcal{W}_0 = \frac{\nu_1 + \nu_2}{2} \quad \text{and} \quad \mathcal{W}_\pi = \frac{\nu_1 - \nu_2}{2}, \tag{4}$$

where

$$\nu_m = \frac{1}{2\pi i}\mathrm{Tr}\ln\left(\bar{P}_A^m \bar{P}_B^{m\dagger}\right) \in \mathbb{Z}, \ \text{with } m = 1, 2.$$

Here, $\bar{P}_{A,B}^m$ represents the polarization operator restricted to the sublattices A and B and defined as $\bar{P}_{A,B}^m = U_{A,B}^{m\dagger} U_{A,B}^\dagger P_x U_{A,B} U_{A,B}^m$ with $P_x = \sum_{x=1,\alpha}^N c_{x,\alpha}^\dagger \exp(-2\pi i x/N_x) c_{x,\alpha}$ [103]. Note that $U_{A,B}^m$ and $U_{A,B}$ denote the unitary matrices constructed from the real space eigenvectors of $\mathcal{H}_F$ and $\mathcal{S}$ respectively.

We implement the periodic drive into two topologically trivial regions of the static phase diagram (see SM [101] for the static phase diagram and number of zero-energy end localized modes): (i) one without the presence of any zero-energy modes and (ii) one hosting only nontopological AZMs [18]. In Figs. 2(a) and 2(b), we illustrate the variation of $\mathcal{W}_0$ and $\mathcal{W}_\pi$ in the V_0-Ω plane for the case (i), where nonzero integer values of $\mathcal{W}_0$ and $\mathcal{W}_\pi$ indicate the number of 0- and π-FMEM pairs, respectively. In the low frequency regime, the driven system hosts multiple FMEMs ($\mathcal{W}_0, \mathcal{W}_\pi > 1$), as the static model band width is much larger than the width of the first Floquet zone. To corroborate with the DWNs, we compute the quasienergy spectrum $\{E_\alpha\}$ by diagonalizing the Floquet Hamiltonian, $\mathcal{H}_F$, under both open (OBC) and periodic (PBC) boundary conditions. The insets of Figs. 2(a) and 2(b) display E_α/Ω as a function of Ω for $V_0 = 2$, confirming the emergence of 0- and π-FMEMs at $E_\alpha/\Omega = 0$ and 0.5, respectively. Specifically, $\mathcal{W}_0 = 1$ and 2 correspond to two and four 0-FMEMs, respectively, localized at the ends of the nanowire as confirmed by the eigenvalue spectrum and site-resolved local density of states (see SM [101] for details). These findings establish the generation of 0- and π-FMEMs driving the trivial static phase of the AM-SC heterostructure.

To investigate the aftermath of nontopological AZMs [18] under periodic drive, we depict the variation of $\mathcal{W}_0$ and $\mathcal{W}_\pi$ in Figs. 2(c) and 2(d), respectively starting from the regime (ii) of the static model. In Fig. 2(c), $\mathcal{W}_0$ is zero for any values of V_0 and Ω implying the absence of topological 0-FMEMs. Notably, for $V_0 = 2$ and $1 < \Omega < 2$ of the drive, zero-energy

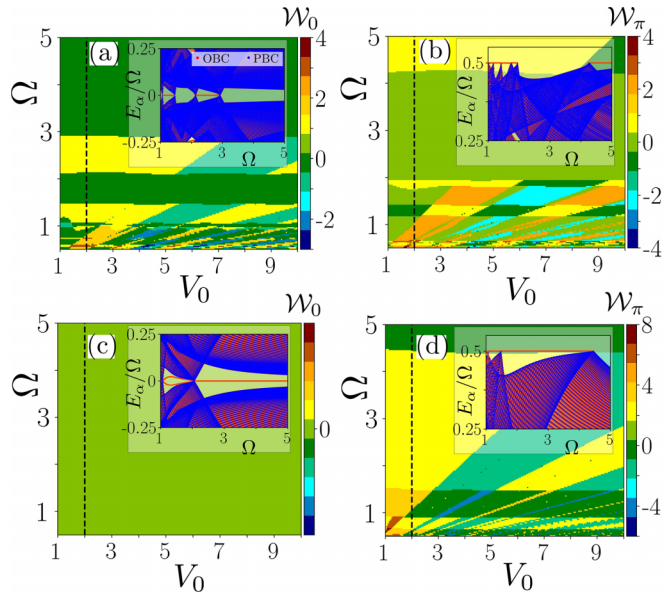

FIG. 2. Illustration of DWNs and the quasienergy spectrum. In panels (a) and (b), we depict the DWNs, $\mathcal{W}_0$ and $\mathcal{W}_\pi$ in the V_0-Ω plane when the static model is in the trivial phase and does not host any zero-energy modes, while panels (c) and (d) showcase the same when the static model hosts AZMs (see SM [101] for the static winding number of the undriven system). The inset of each panel displays the quasienergy spectrum, E_α/Ω, as a function of Ω (along the vertical dashed lines of each panel) for $V_0 = 2$ employing both OBC and PBC, highlighting the emergence of 0-FMEMs [inset of (a) and (c)] and π-FMEMs [inset of (b) and (d)]. We choose the model parameters as $(\mu/t, J_A/t = 1.5, 0.4)$ in panels (a) and (b) and $(\mu/t, J_A/t = 0, 1.2)$ in panels (c) and (d) while we consider a finite size system with $N_x = 100$ lattice sites across all the panels.

AZMs are gapped out as shown in the inset of Fig. 2(c). However, AZMs still persist for large Ω, reminiscent of AZMs in the static Hamiltonian. Despite the absence of 0-FMEMs, in Fig. 2(d) we observe $\mathcal{W}_\pi$ to inherit even integer values implying the presence of multiple π-FMEMs, which we coin as "TAZMs" as they emerge by driving the trivial AZMs. The quasienergy spectrum, E_α/Ω, depicted as a function of Ω, clearly reveals the appearance of π-FMEMs at $E_\alpha/\Omega = 0.5$ [see inset of Fig. 2(d)]. These results confirm that Floquet driving can eliminate nontopological AZMs while inducing robust topological π-FMEMs, addressing the first key question of our Letter.

For a comprehensive analysis, we calculate the bulk gap associated with 0- and π-FMEMs, which supports the DWN phase diagram (see SM [101] for details). Moreover, we investigate the robustness of DWNs against static onsite random disorder and find that π-FMEMs turn out to be more robust compared to the 0-FMEMs (see SM [101] for further details).

Josephson current signature of static MZMs/AZMs. To answer the second question, we consider a JJ formed by two weakly coupled TSCs with coupling strength $\tilde{t}$ and a phase difference $\phi_L - \phi_R = \phi$ between them as shown in Fig. 1(b). Here, each TSC corresponds to our 1D RNW with proximity induced AM and SC. First, we switch off the periodic drive and investigate the JC in the static case to distinguish between MZMs and AZMs as proposed in the static Hamiltonian [18].

The Hamiltonian of the JJ is constructed as

$$\mathcal{H}_{\rm JJ} = \mathcal{H}_0^L + \mathcal{H}_0^R + \mathcal{H}^{LR}, \tag{5}$$

where

$$\mathcal{H}_0^\alpha = \sum_{x,x'=1}^{N_x} \Psi_x^{\alpha\dagger} H_{x,x'}^\alpha(\phi_\alpha)\Psi_{x'}^\alpha, \quad \alpha = L, R,$$
$$\mathcal{H}^{LR} = \Psi_{N_x}^{L\dagger}\left[\frac{\tilde{t}}{2}\,\pi_z\sigma_0\right]\Psi_1^R + \text{H.c.} \tag{6}$$

Here, $\Psi_x^\alpha(\Psi_x^{\alpha\dagger})$ corresponds to the annihilation (creation) operator of the electron at site x in the left ($\alpha = L$) and right ($\alpha = R$) SC. Also, $H_{x,x'}^{L/R}(\phi_{L/R})$ represents the Hamiltonian for the left/right TSCs, governed by the Eq. (1) with superconducting phase $\phi_{L/R}$. The third term, $\mathcal{H}^{LR}$, denotes the coupling between the last site of the left SC and first site of the right SC. For the purpose of our Letter, we consider two situations when each TSC hosts either topological MZMs or nontopological AZMs at its ends.

We compute the JC, $I(\phi)$, flowing across the junction in the presence of phase bias, ϕ, following the relation [104,105]

$$I(\phi) = \sum_\beta f_{\rm FD}(\epsilon_\beta)\frac{\partial\epsilon_\beta(\phi)}{\partial\phi}, \tag{7}$$

where $f_{\rm FD}(\epsilon_\beta)$ denotes the Fermi-Dirac distribution function representing the occupation probability of the βth energy eigenstate with energy ϵ_β. In the zero temperature limit, the summation in Eq. (7) involves only the negative energy eigenvalues, i.e., $\epsilon_\beta \leqslant 0$.

We investigate the influence of phase bias ϕ on $\epsilon_\beta(\phi)$ for MZMs and AZMs localized near and far from the junction in Fig. 3(a). Due to the coupling, $\tilde{t}$, between the TSCs, the modes localized near the junction [blue spikes in Fig. 1(b)] hybridize, forming finite energy quasiparticle states. In contrast, the zero modes far from the junction [red spikes in Fig. 1(b)] remain at zero energy as shown in Fig. 3(a), provided $N_x \gg \xi_M$ where ξ_M is the Majorana localization length. Interestingly, the junction localized MZMs follow $\epsilon_\pm^{\rm jun}(\phi) \propto \pm\cos(\phi/2)$ leading to energy crossing at $\phi = \pi$ which signals a switching of the ground-state fermion parity resulting in the emergence of the 4π-periodic Josephson effect [3,4,6]. In sharp contrast, junction localized AZMs, though ϕ dependent [see inset of Fig. 3(a)], do not exhibit any energy crossing which indicates no change in fermion parity and confirms their nontopological nature, though predicted to be topological in Ref. [49]. In Fig. 3(b), we depict the behavior of static JC $I(\phi)$ for both AZMs and MZMs where for MZMs, a clear discontinuity at $\phi = \pi$ reflects 4π periodicity, while for AZMs, $I(\phi)$ is 2π periodic with a maximum at $\phi = \pi/2$. This distinct behavior in JC offers a clear signature to distinguish the AZMs from MZMs (apart from dI/dV and shot noise signature [18]), thus addressing our second key question. We also introduce a random static onsite disorder in the Hamiltonian $\mathcal{H}_{\rm dis} = \sum_x \Psi_x^\dagger[V(x)\pi_z\sigma_0]\Psi_x$ where $V(x)$ is a random number uniformly distributed in the range $[-V_{\rm dis}/2, V_{\rm dis}/2]$. We present the effect of disorder on the JC for both MZMs and AZMs in Figs. 3(c) and 3(d), respectively. For MZMs, the discontinuity at $\phi = \pi$ diminishes with increasing disorder strength and for strong disorder, the 4π periodic nature is governed by conventional 2π-periodic JC [see inset of Fig. 3(c)]. On the other hand, in case of AZMs, disorder suppresses the JC amplitude without altering its periodicity.

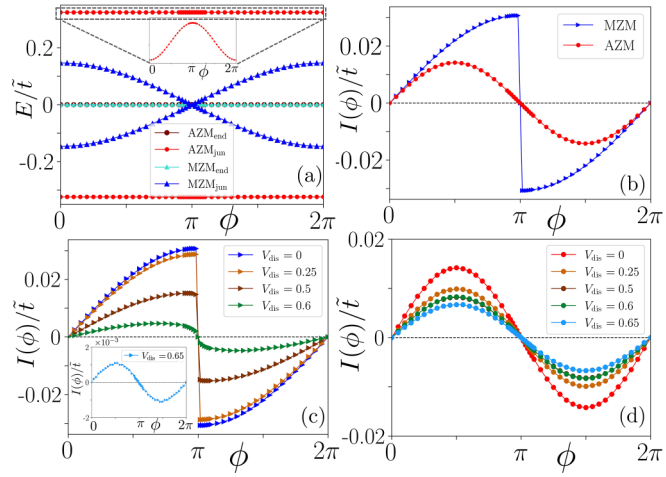

FIG. 3. Behavior of JC flowing across the static JJ. In panel (a), we present the $\epsilon - \phi$ relation due to MZMs and AZMs localized near ($\text{AZM}_{\rm jun}$, $\text{MZM}_{\rm jun}$) and far from the junction ($\text{AZM}_{\rm end}$, $\text{MZM}_{\rm end}$). In panel (b), we depict the variation of JC, $I(\phi)$ as a function of ϕ for MZMs and AZMs. Panels (c) and (d) display the effect of disorder on $I(\phi)$ for different disorder strengths, $V_{\rm dis}$, corresponding to MZMs and AZMs, respectively. For MZMs, we choose $(\mu, J_A) = (1.1t, 0.4t)$, while for AZMs $(\mu, J_A) = (0, 1.2t)$. We fix the system size $N_x = 340$ lattice sites and $\tilde{t} = 0.01t$ in all panels. We consider 50 disorder configurations in panels (c) and (d).

Josephson current signature of FMEMs/TAZMs. Here, we apply identical time-periodic drive $V(t)$ [Eq. (2)] to both the TSCs in the JJ setup as illustrated in Fig. 1(b) to investigate Floquet JC signatures of FMEMs. The Floquet drive carries the system into an out-of-equilibrium phase where the occupation of quasienergy states deviates from the equilibrium distribution. When such a driven system is weakly coupled to a thermal reservoir at temperature θ_r and chemical potential μ_r, the steady-state occupation of a quasienergy state, E_α, is governed by [95]

$$n(E_\alpha, \mu_r) = \sum_{m\in\mathbb{Z}} \langle u_\alpha^{(m)}|u_\alpha^{(m)}\rangle f_{\rm FD}(E_\alpha + m\Omega - \mu_r), \tag{8}$$

where $|u_\alpha^{(m)}\rangle$ are the Fourier modes of $|\varphi_\alpha(t)\rangle$, i.e., $|\varphi_\alpha(t)\rangle = \sum_{m\in\mathbb{Z}} e^{-im\Omega t}|u_\alpha^{(m)}\rangle$. Importantly, Eq. (8) allows energy resolved probing of the 0- and π-FMEMs by setting $\mu_r^0 = n\Omega$ and $\mu_r^\pi = (n + 1/2)\Omega$, respectively with $n \in \mathbb{Z}$. The JC, averaged over the full time cycle, is computed utilizing the relation [95] (see SM [101] for brief derivation)

$$I_{0/\pi}(\phi) = \sum_\alpha n\big(E_\alpha, \mu_r^{0/\pi}\big)\frac{\partial E_\alpha(\phi)}{\partial\phi}. \tag{9}$$

Note that performing brute force derivatives of $E_\alpha(\phi)$, without invoking the correct occupation number, may produce a discontinuous jump in JC at $\phi = \pi$ [106], but fails to distinguish between the presence of 0- and π-FMEMs (see SM [101] for further details). Crucially, even when FMEMs are present, the

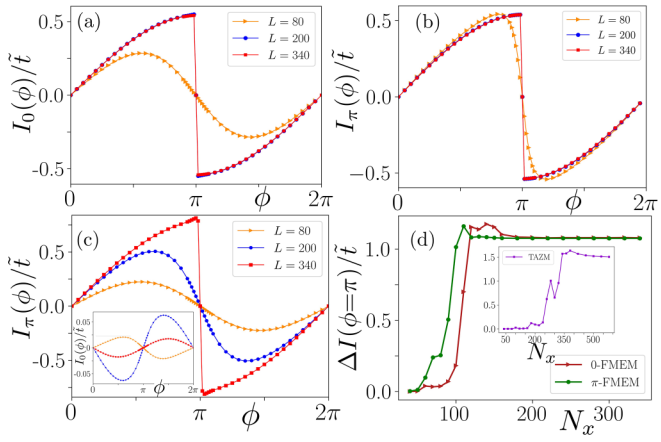

FIG. 4. Variation of Floquet JC across the driven JJ. In panels (a) and (b), we present the variation of JC when the driven system hosts only 0-FMEMs and only π-FMEMs, respectively. On the other hand, panel (c) (inset) illustrates the JC for TAZMs (zero-energy Floquet AZMs) for various system sizes. Panel (d) highlights the discontinuous jump in JC at $\phi = \pi$ as a function of N_x corresponding to panels (a) and (b) while the inset represents the discontinuity for TAZMs as presented in panel (c). The model parameters in (μ, J_A, Ω, V_0) space are chosen as (a) $(1.5t, 0.4t, 2.4, 4.2t)$, (b) $(1.5t, 0.4t, 4.8, 4.5t)$, and (c) $(0, 1.2t, 3, 3.1t)$ and $\tilde{t} = 0.01t$ in all the panels.

4π periodicity in $I(\phi)$ emerges only if $N_x \gg \xi_m$. Otherwise, a conventional 2π-periodic Josephson effect is restored due to overlap between the modes localized near and far from the junction (see SM [101] for details).

We compute $I_{0/\pi}(\phi)$ corresponding to three phases of the driven system hosting (i) only 0-FMEMs [Fig. 4(a)], (ii) only π-FMEMs [Fig. 4(b)], and (iii) multiple π-FMEMs (TAZMs) with nontopological AZMs at $E_\alpha = 0$ [Fig. 4(c)] considering various lengths of TSCs. In cases (i) and (ii), we observe the 4π-periodic Josephson effect in $I_0(\phi)$ and $I_\pi(\phi)$ respectively when $N_x \gg \xi_M$. Interestingly, in case (iii) only $I_\pi(\phi)$ exhibits a discontinuous jump at $\phi = \pi$, however $I_0(\phi)$ remains 2π periodic [see inset of Fig. 4(c)] even if we increase the length of the two TSCs, highlighting the nontopological nature of Floquet AZMs that remain at high frequency. The crossover from 2π to 4π periodicity is clearly visible with increasing the system size as captured by the discontinuos jump in $\Delta I(\phi = \pi)$ [see Fig. 4(d)]. The critical length N_x^c for such crossover is governed by the Majorana localization length ξ_M. Although the latter varies with model parameters, for cases (i) and (ii) $N_x^c \simeq 100$ while for TAZMs $N_x^c \simeq 300$. Physically, such different length scales can be attributed to the corresponding size of the π gap protecting the FMEMs and TAZMs. Additionally, the 4π-periodic Josephson effect can only distinguish the topological modes from the nontopological ones. However, it cannot differentiate between two topological phases, e.g., between $\mathcal{W}_0 = 1$ and 2 with any universal feature, since in both cases JC remains 4π periodic (see SM [101] for details) via the discontinous jump at $\phi = \pi$. These results establish that the TAZMs, obtained by periodically driving the phase hosting AZMs, exhibit the hallmark 4π-periodic Josephson effect, answering our final key question.

Summary and discussion. To summarize, in this Letter, we periodically drive a heterostructure consisting of a 1D RNW proximitized to a bulk s-wave SC and d-wave AM to generate FMEMs from the nontopological regime of the static phase. Topological characterization employing DWNs $\mathcal{W}_0$ and $\mathcal{W}_\pi$ reveals a rich phase diagram hosting multiple 0- and π-FMEMs. Crucially, nontopological AZMs can be gapped out by the drive, while inducing multiple π-FMEMs, termed as TAZMs, inheriting topological properties. Note that, in the high frequency limit, the system hosts nontopological zero-energy AZMs reminiscent of the static AZMs. To distinguish between MZMs and AZMs, we choose a JJ setup of two weakly coupled TSCs. While MZMs exhibit a 4π periodicity in JC due to fermion parity switching at $\phi = \pi$, for AZMs JC remains 2π periodic, confirming their nontopological nature. Extending this to the driven system, we use energy-resolved Floquet JC formalism [95] to identify 0- and π-FMEMs via 4π-periodic signatures. Intriguingly, TAZMs also display discontinuities in the JC, revealing 4π periodicity at sufficiently larger system sizes owing to large localization length (smaller π gap). Our results establish a robust framework to engineer, detect, and distinguish dynamical topological modes utilizing Floquet JC. Generation of FMEMs in planar Josephson junctions using a time-periodic gate voltage at the barrier region was reported in Ref. [91]. However, instead of computing JC, they relied on dI/dV and density of states to probe the FMEMs.

In addition to better proximity effect due to zero net magnetization, the use of an AM instead of external Zeeman field can offer further advantages in both static and driven systems. In the static case, the bulk topological superconducting gap is significantly enhanced in the altermagnetic heterostructure, sometimes even twice the bulk gap obtained with the Zeeman field, providing better stability against disorder in comparision with the heterostructure with external magnetic field. Moreover, the enhnaced bulk gap leads to an enhanced temperature range, below which Majorana modes are possible to observe in experiments. Furthermore, in driven systems, the AM extends the topological phase boundary beyond the phase boundary obtained with the Zeeman field leading to an enlarged parameter space for the realization of FMEMs. We refer to the SM [101] for the detailed discussion.

As far as experimental detection of the 4π-periodic Josephson effect is concerned, this may face key challenges: (i) quasiparticle poisoning, where external tunneling processes from attached leads can alter the fermion parity and restore the conventional 2π periodicity [6,19], and (ii) Landau-Zener tunneling wherein a highly transparent 2π-periodic state can tunnel through the avoided crossing at $\phi = \pi$, mimicking the 4π-periodic Josephson effect [107,108]. To circumvent these challenges, experimental detection often relies on the ac Josephson effect, where the appearance of only even-integer Shapiro steps indicates topological superconductivity [19,108]. However, experimental progress to detect FMEMs in periodically driven JJs still remains in its infancy [109]. Concerning the realistic physical microscopic model parameters, in our calculations we have scaled all the energy scales in units of strength of hopping amplitude, t, instead of considering actual values corresponding to real materials. However, we propose an estimate of the parameter values

from our numerical simulation (not based on real materials) for which the intriguing features of our system appear. A representative set of parameter values is as follows: $t \simeq 1\,\text{meV}$ (suppose given for any nanowire material), and then other parameters are $\Delta_0 \simeq 300\,\mu\text{eV}$, $\lambda_R \simeq 500\,\mu\text{eV}$, $J_A = 0.5\text{–}1\,\text{meV}$, $V_0 \leqslant 2.5\,\text{meV}$, and $\Omega \approx 40\,\text{GHz}$. Moreover, in future, one can explore ac Josephson signatures in driven systems to distinguish trivial zero modes from topological Majorana modes. Furthermore, employing numerous driving protocols, one may also explore the possibility of complete elimination of AZMs from this hybrid setup.

Acknowledgments. We acknowledge Arijit Kundu and Rekha Kumari for stimulating discussions. A.P., D.M., and A.S. acknowledge SAMKHYA: High-Performance Computing Facility provided by Institute of Physics, Bhubaneswar and the two workstations provided by Institute of Physics, Bhubaneswar from the DAE APEX Project, for numerical computations. T.N. acknowledges NFSG BITS Pilani Grant No. NFSG/HYD/2023/H0911.

Data availability. The data that support the findings of this article are not publicly available. The data are available from the authors upon reasonable request.

[1] A. Y. Kitaev, Unpaired Majorana fermions in quantum wires, Phys. Usp. **44**, 131 (2001).
[2] M. Leijnse and K. Flensberg, Introduction to topological superconductivity and Majorana fermions, Semicond. Sci. Technol. **27**, 124003 (2012).
[3] J. Alicea, Y. Oreg, G. Refael, F. von Oppen, and M. P. A. Fisher, Non-Abelian statistics and topological quantum information processing in 1D wire networks, Nat. Phys. **7**, 412 (2011).
[4] J. Alicea, New directions in the pursuit of Majorana fermions in solid state systems, Rep. Prog. Phys. **75**, 076501 (2012).
[5] R. M. Lutchyn, J. D. Sau, and S. D. Sarma, Majorana fermions and a topological phase transition in semiconductor-superconductor heterostructures, Phys. Rev. Lett. **105**, 077001 (2010).
[6] C. Beenakker, Search for Majorana fermions in superconductors, Annu. Rev. Condens. Matter Phys. **4**, 113 (2013).
[7] S. Tewari and J. D. Sau, Topological invariants for spin-orbit coupled superconductor nanowires, Phys. Rev. Lett. **109**, 150408 (2012).
[8] A. Kitaev, Fault-tolerant quantum computation by anyons, Ann. Phys. (NY) **303**, 2 (2003).
[9] C. Nayak, S. H. Simon, A. Stern, M. Freedman, and S. D. Sarma, Non-Abelian anyons and topological quantum computation, Rev. Mod. Phys. **80**, 1083 (2008).
[10] X.-L. Qi and S.-C. Zhang, Topological insulators and superconductors, Rev. Mod. Phys. **83**, 1057 (2011).
[11] R. Aguado, Majorana quasiparticles in condensed matter, Riv. Nuovo Cimento **40**, 523 (2017).
[12] A. Yazdani, F. von Oppen, B. I. Halperin, and A. Yacoby, Hunting for Majoranas, Science **380**, eade0850 (2023).
[13] P. Chatterjee, S. Pradhan, A. K. Nandy, and A. Saha, Tailoring the phase transition from topological superconductor to trivial superconductor induced by magnetic textures of a spin chain on a *p*-wave superconductor, Phys. Rev. B **107**, 085423 (2023).
[14] Z. Yan, Majorana corner and hinge modes in second-order topological insulator/superconductor heterostructures, Phys. Rev. B **100**, 205406 (2019).
[15] C. Wang, F. Liu, and H. Huang, Effective model for fractional topological corner modes in quasicrystals, Phys. Rev. Lett. **129**, 056403 (2022).
[16] M. Subhadarshini, A. Pal, P. Chatterjee, and A. Saha, Multiple topological phase transitions unveiling gapless topological superconductivity in magnet/unconventional superconductor hybrid platform, Appl. Phys. Lett. **124**, 183102 (2024).
[17] K. T. Law, P. A. Lee, and T. K. Ng, Majorana fermion induced resonant Andreev reflection, Phys. Rev. Lett. **103**, 237001 (2009).
[18] D. Mondal, A. Pal, A. Saha, and T. Nag, Distinguishing between topological Majorana and trivial zero modes via transport and shot noise study in an altermagnet heterostructure, Phys. Rev. B **111**, L121401 (2025).
[19] L. P. Rokhinson, X. Liu, and J. K. Furdyna, The fractional a.c. Josephson effect in a semiconductor-superconductor nanowire as a signature of Majorana particles, Nat. Phys. **8**, 795 (2012).
[20] A. D. K. Finck, D. J. Van Harlingen, P. K. Mohseni, K. Jung, and X. Li, Anomalous modulation of a zero-bias peak in a hybrid nanowire-superconductor device, Phys. Rev. Lett. **110**, 126406 (2013).
[21] S. M. Albrecht, A. P. Higginbotham, M. Madsen, F. Kuemmeth, T. S. Jespersen, J. Nygård, P. Krogstrup, and C. M. Marcus, Exponential protection of zero modes in Majorana islands, Nature (London) **531**, 206 (2016).
[22] A. Das, Y. Ronen, Y. Most, Y. Oreg, M. Heiblum, and H. Shtrikman, Zero-bias peaks and splitting in an Al-InAs nanowire topological superconductor as a signature of Majorana fermions, Nat. Phys. **8**, 887 (2012).
[23] V. Mourik, K. Zuo, S. M. Frolov, S. R. Plissard, E. P. A. M. Bakkers, and L. P. Kouwenhoven, Signatures of Majorana fermions in hybrid superconductor-semiconductor nanowire devices, Science **336**, 1003 (2012).
[24] M. T. Deng, S. Vaitiekėnas, E. B. Hansen, J. Danon, M. Leijnse, K. Flensberg, J. Nygård, P. Krogstrup, and C. M. Marcus, Majorana bound state in a coupled quantum-dot hybrid-nanowire system, Science **354**, 1557 (2016).
[25] J. Chen, P. Yu, J. Stenger, M. Hocevar, D. Car, S. R. Plissard, E. P. A. M. Bakkers, T. D. Stanescu, and S. M. Frolov, Experimental phase diagram of zero-bias conductance peaks in superconductor/semiconductor nanowire devices, Sci. Adv. **3**, e1701476 (2017).
[26] G. Kells, D. Meidan, and P. W. Brouwer, Near-zero-energy end states in topologically trivial spin-orbit coupled superconducting nanowires with a smooth confinement, Phys. Rev. B **86**, 100503 (2012).
[27] E. J. H. Lee, X. Jiang, M. Houzet, R. Aguado, C. M. Lieber, and S. De Franceschi, Spin-resolved Andreev levels and parity crossings in hybrid superconductor-semiconductor nanostructures, Nat. Nanotechnol. **9**, 79 (2014).
[28] L. S. Ricco, M. de Souza, M. S. Figueira, I. A. Shelykh, and A. C. Seridonio, Spin-dependent zero-bias peak in a hybrid

nanowire-quantum dot system: Distinguishing isolated Majorana fermions from Andreev bound states, Phys. Rev. B **99**, 155159 (2019).

[29] D. Goldhaber-Gordon, H. Shtrikman, D. Mahalu, D. Abusch-Magder, U. Meirav, and M. A. Kastner, Kondo effect in a single-electron transistor, Nature (London) **391**, 156 (1998).

[30] S. M. Cronenwett, T. H. Oosterkamp, and L. P. Kouwenhoven, A tunable Kondo effect in quantum dots, Science **281**, 540 (1998).

[31] D. Bagrets and A. Altland, Class *D* spectral peak in Majorana quantum wires, Phys. Rev. Lett. **109**, 227005 (2012).

[32] L. Fu and C. L. Kane, Josephson current and noise at a superconductor/quantum-spin-Hall-insulator/superconductor junction, Phys. Rev. B **79**, 161408 (2009).

[33] K. T. Law and P. A. Lee, Robustness of Majorana fermion induced fractional Josephson effect in multichannel superconducting wires, Phys. Rev. B **84**, 081304 (2011).

[34] C.-K. Chiu and S. D. Sarma, Fractional Josephson effect with and without Majorana zero modes, Phys. Rev. B **99**, 035312 (2019).

[35] F. Crépin and B. Trauzettel, Parity measurement in topological Josephson junctions, Phys. Rev. Lett. **112**, 077002 (2014).

[36] P. Marra, R. Citro, and A. Braggio, Signatures of topological phase transitions in Josephson current-phase discontinuities, Phys. Rev. B **93**, 220507 (2016).

[37] J. Cayao, E. Prada, P. San-Jose, and R. Aguado, SNS junctions in nanowires with spin-orbit coupling: Role of confinement and helicity on the subgap spectrum, Phys. Rev. B **91**, 024514 (2015).

[38] J. Cayao, P. San-Jose, A. M. Black-Schaffer, R. Aguado, and E. Prada, Majorana splitting from critical currents in Josephson junctions, Phys. Rev. B **96**, 205425 (2017).

[39] O. A. Awoga, J. Cayao, and A. M. Black-Schaffer, Supercurrent detection of topologically trivial zero-energy states in nanowire junctions, Phys. Rev. Lett. **123**, 117001 (2019).

[40] L. Šmejkal, J. Sinova, and T. Jungwirth, Beyond conventional ferromagnetism and antiferromagnetism: A phase with nonrelativistic spin and crystal rotation symmetry, Phys. Rev. X **12**, 031042 (2022).

[41] L. Šmejkal, J. Sinova, and T. Jungwirth, Emerging research landscape of altermagnetism, Phys. Rev. X **12**, 040501 (2022).

[42] S. Bhowal and N. A. Spaldin, Ferroically ordered magnetic octupoles in *d*-wave altermagnets, Phys. Rev. X **14**, 011019 (2024).

[43] H. Bai, Y. C. Zhang, Y. J. Zhou, P. Chen, C. H. Wan, L. Han, W. X. Zhu, S. X. Liang, Y. C. Su, X. F. Han, F. Pan, and C. Song, Efficient spin-to-charge conversion via altermagnetic spin splitting effect in antiferromagnet RuO_2, Phys. Rev. Lett. **130**, 216701 (2023).

[44] I. I. Mazin, Altermagnetism in MnTe: Origin, predicted manifestations, and routes to detwinning, Phys. Rev. B **107**, L100418 (2023).

[45] X. Zhou, W. Feng, R.-W. Zhang, L. Šmejkal, J. Sinova, Y. Mokrousov, and Y. Yao, Crystal thermal transport in altermagnetic RuO_2, Phys. Rev. Lett. **132**, 056701 (2024).

[46] H.-J. Lin, S.-B. Zhang, H.-Z. Lu, and X. C. Xie, Coulomb drag in altermagnets, Phys. Rev. Lett. **134**, 136301 (2025).

[47] S. Lee, S. Lee, S. Jung, J. Jung, D. Kim, Y. Lee, B. Seok, J. Kim, B. G. Park, L. Šmejkal, C.-J. Kang, and C. Kim, Broken Kramers degeneracy in altermagnetic MnTe, Phys. Rev. Lett. **132**, 036702 (2024).

[48] B. Jiang, M. Hu, J. Bai, Z. Song, C. Mu, G. Qu, W. Li, W. Zhu, H. Pi, Z. Wei, Y.-J. Sun, Y. Huang, X. Zheng, Y. Peng, L. He, S. Li, J. Luo, Z. Li, G. Chen, H. Li *et al.*, A metallic room-temperature d-wave altermagnet, Nat. Phys. **21**, 754 (2025).

[49] S. A. A. Ghorashi, T. L. Hughes, and J. Cano, Altermagnetic routes to Majorana modes in zero net magnetization, Phys. Rev. Lett. **133**, 106601 (2024).

[50] Y.-X. Li and C.-C. Liu, Majorana corner modes and tunable patterns in an altermagnet heterostructure, Phys. Rev. B **108**, 205410 (2023).

[51] Y.-X. Li, Y. Liu, and C.-C. Liu, Creation and manipulation of higher-order topological states by altermagnets, Phys. Rev. B **109**, L201109 (2024).

[52] D. Zhu, Z.-Y. Zhuang, Z. Wu, and Z. Yan, Topological superconductivity in two-dimensional altermagnetic metals, Phys. Rev. B **108**, 184505 (2023).

[53] Y.-X. Li, Realizing tunable higher-order topological superconductors with altermagnets, Phys. Rev. B **109**, 224502 (2024).

[54] S.-B. Zhang, L.-H. Hu, and T. Neupert, Finite-momentum Cooper pairing in proximitized altermagnets, Nat. Commun. **15**, 1801 (2024).

[55] Z. Yin, H. Li, Z. Yan, and S. Wan, Multifold Majorana corner modes arising from multiple pairs of helical edge states, Phys. Rev. B **111**, 085421 (2025).

[56] Y. Fukaya, B. Lu, K. Yada, Y. Tanaka, and J. Cayao, Superconducting phenomena in systems with unconventional magnets, J. Phys.: Condens. Matter **37**, 313003 (2025).

[57] K. Maeda, Y. Fukaya, K. Yada, B. Lu, Y. Tanaka, and J. Cayao, Classification of pair symmetries in superconductors with unconventional magnetism, Phys. Rev. B **111**, 144508 (2025).

[58] P. Chatterjee and V. Juričić, Interplay between altermagnetism and topological superconductivity in an unconventional superconducting platform, Phys. Rev. B **112**, 054503 (2025).

[59] Y.-X. Li, Y. Liu, and C.-C. Liu, Tunable topological superconductivity by fully compensated ferrimagnets, arXiv:2504.19844.

[60] B. Lu, K. Maeda, H. Ito, K. Yada, and Y. Tanaka, φ Josephson junction induced by altermagnetism, Phys. Rev. Lett. **133**, 226002 (2024).

[61] Y. Fukaya, K. Maeda, K. Yada, J. Cayao, Y. Tanaka, and B. Lu, Josephson effect and odd-frequency pairing in superconducting junctions with unconventional magnets, Phys. Rev. B **111**, 064502 (2025).

[62] H.-P. Sun, S.-B. Zhang, C.-A. Li, and B. Trauzettel, Tunable second harmonic in altermagnetic Josephson junctions, Phys. Rev. B **111**, 165406 (2025).

[63] J. A. Ouassou, A. Brataas, and J. Linder, Dc Josephson effect in altermagnets, Phys. Rev. Lett. **131**, 076003 (2023).

[64] T. Oka and H. Aoki, Photovoltaic Hall effect in graphene, Phys. Rev. B **79**, 081406 (2009).

[65] T. Mikami, S. Kitamura, K. Yasuda, N. Tsuji, T. Oka, and H. Aoki, Brillouin-Wigner theory for high-frequency expansion in periodically driven systems: Application to Floquet topological insulators, Phys. Rev. B **93**, 144307 (2016).

[66] N. H. Lindner, G. Refael, and V. Galitski, Floquet topological insulator in semiconductor quantum wells, Nat. Phys. **7**, 490 (2011).

[67] M. S. Rudner, N. H. Lindner, E. Berg, and M. Levin, Anomalous edge states and the bulk-edge correspondence for periodically driven two-dimensional systems, Phys. Rev. X **3**, 031005 (2013).

[68] G. Usaj, P. M. Perez-Piskunow, L. E. F. F. Torres, and C. A. Balseiro, Irradiated graphene as a tunable Floquet topological insulator, Phys. Rev. B **90**, 115423 (2014).

[69] J. K. Asbóth, B. Tarasinski, and P. Delplace, Chiral symmetry and bulk-boundary correspondence in periodically driven one-dimensional systems, Phys. Rev. B **90**, 125143 (2014).

[70] P. M. Perez-Piskunow, G. Usaj, C. A. Balseiro, and L. E. F. F. Torres, Floquet chiral edge states in graphene, Phys. Rev. B **89**, 121401 (2014).

[71] A. Eckardt and E. Anisimovas, High-frequency approximation for periodically driven quantum systems from a Floquet-space perspective, New J. Phys. **17**, 093039 (2015).

[72] T. Oka and S. Kitamura, Floquet engineering of quantum materials, Annu. Rev. Condens. Matter Phys. **10**, 387 (2019).

[73] S. Yao, Z. Yan, and Z. Wang, Topological invariants of Floquet systems: General formulation, special properties, and Floquet topological defects, Phys. Rev. B **96**, 195303 (2017).

[74] M. S. Rudner and N. H. Lindner, Band structure engineering and non-equilibrium dynamics in Floquet topological insulators, Nat. Rev. Phys. **2**, 229 (2020).

[75] T. Nag and B. Roy, Anomalous and normal dislocation modes in Floquet topological insulators, Commun. Phys. **4**, 157 (2021).

[76] M. Benito, A. Gómez-León, V. M. Bastidas, T. Brandes, and G. Platero, Floquet engineering of long-range p-wave superconductivity, Phys. Rev. B **90**, 205127 (2014).

[77] A. K. Ghosh, T. Nag, and A. Saha, Floquet generation of a second-order topological superconductor, Phys. Rev. B **103**, 045424 (2021).

[78] A. K. Ghosh, T. Nag, and A. Saha, Floquet second order topological superconductor based on unconventional pairing, Phys. Rev. B **103**, 085413 (2021).

[79] A. K. Ghosh, G. C. Paul, and A. Saha, Higher order topological insulator via periodic driving, Phys. Rev. B **101**, 235403 (2020).

[80] A. K. Ghosh, T. Nag, and A. Saha, Dynamical construction of quadrupolar and octupolar topological superconductors, Phys. Rev. B **105**, 155406 (2022).

[81] A. K. Ghosh, T. Nag, and A. Saha, Generation of higher-order topological insulators using periodic driving, J. Phys.: Condens. Matter **36**, 093001 (2024).

[82] A. K. Ghosh, T. Nag, and A. Saha, Floquet second-order topological Anderson insulator hosting corner localized modes, Phys. Rev. B **110**, 125427 (2024).

[83] A. K. Ghosh, R. Arouca, and A. M. Black-Schaffer, Local and energy-resolved topological invariants for Floquet systems, Phys. Rev. B **110**, 245306 (2024).

[84] S. Kohler, J. Lehmann, and P. Hänggi, Driven quantum transport on the nanoscale, Phys. Rep. **406**, 379 (2005).

[85] M. Thakurathi, A. A. Patel, D. Sen, and A. Dutta, Floquet generation of Majorana end modes and topological invariants, Phys. Rev. B **88**, 155133 (2013).

[86] M. Thakurathi, D. Loss, and J. Klinovaja, Floquet Majorana fermions and parafermions in driven Rashba nanowires, Phys. Rev. B **95**, 155407 (2017).

[87] A. C. Potter, T. Morimoto, and A. Vishwanath, Classification of interacting topological Floquet phases in one dimension, Phys. Rev. X **6**, 041001 (2016).

[88] A. Kundu and B. Seradjeh, Transport signatures of Floquet Majorana fermions in driven topological superconductors, Phys. Rev. Lett. **111**, 136402 (2013).

[89] A. Farrell and T. Pereg-Barnea, Photon-inhibited topological transport in quantum well heterostructures, Phys. Rev. Lett. **115**, 106403 (2015).

[90] A. Farrell and T. Pereg-Barnea, Edge-state transport in Floquet topological insulators, Phys. Rev. B **93**, 045121 (2016).

[91] D. T. Liu, J. Shabani, and A. Mitra, Floquet Majorana zero and π modes in planar Josephson junctions, Phys. Rev. B **99**, 094303 (2019).

[92] D. Mondal, A. K. Ghosh, T. Nag, and A. Saha, Topological characterization and stability of Floquet Majorana modes in rashba nanowires, Phys. Rev. B **107**, 035427 (2023).

[93] D. Mondal, A. K. Ghosh, T. Nag, and A. Saha, Engineering anomalous Floquet Majorana modes and their time evolution in a helical Shiba chain, Phys. Rev. B **108**, L081403 (2023).

[94] D. Mondal, R. Kumari, T. Nag, and A. Saha, Transport signatures of single and multiple Floquet Majorana modes in a one-dimensional Rashba nanowire and Shiba chain, Phys. Rev. B **111**, 235441 (2025).

[95] R. Kumari, B. Seradjeh, and A. Kundu, Josephson-current signatures of unpaired Floquet Majorana fermions, Phys. Rev. Lett. **133**, 196601 (2024).

[96] C.-K. Chiu, J. C. Y. Teo, A. P. Schnyder, and S. Ryu, Classification of topological quantum matter with symmetries, Rev. Mod. Phys. **88**, 035005 (2016).

[97] A. Eckardt, *Colloquium*: Atomic quantum gases in periodically driven optical lattices, Rev. Mod. Phys. **89**, 011004 (2017).

[98] M. Suzuki, Generalized trotter's formula and systematic approximants of exponential operators and inner derivations with applications to many-body problems, Commun. Math. Phys. **51**, 183 (1976).

[99] H. De Raedt and B. De Raedt, Applications of the generalized Trotter formula, Phys. Rev. A **28**, 3575 (1983).

[100] T. Qin, P. Zhang, and G. Yang, Nondiagonal disorder enhanced topological properties of graphene with laser irradiation, Phys. Rev. B **105**, 184203 (2022).

[101] See Supplemental Material at http://link.aps.org/supplemental/10.1103/prnx-47mk for detailed discussions on the real space formalism of the dynamical winding number, quasienergy spectra, and LDOS of 0- and π-FMEMs, analysis of bulk gaps in the driven system, advantages of using altermagnets over external Zeeman field, stability of the driven topological

superconductor against disorder, Floquet Josephson current via numerical exact diagonalization, brief derivation of the Floquet Josephson current formalism, Floquet Josephson current for $\mathcal{W}_0 = 1$ and 2, and local density of states and energy deviation of topological accidental zero modes in driven Josephson junctions.

[102] W. A. Benalcazar and A. Cerjan, Chiral-symmetric higher-order topological phases of matter, Phys. Rev. Lett. **128**, 127601 (2022).

[103] R. Resta, Quantum-mechanical position operator in extended systems, Phys. Rev. Lett. **80**, 1800 (1998).

[104] C. W. J. Beenakker, Universal limit of critical-current fluctuations in mesoscopic Josephson junctions, Phys. Rev. Lett. **67**, 3836 (1991).

[105] H.-J. Kwon, K. Sengupta, and V. M. Yakovenko, Fractional ac Josephson effect in p- and d-wave superconductors, Eur. Phys. J. B **37**, 349 (2003).

[106] K. Roy, G. Paul, D. Debnath, K. Bhattacharyya, and S. Basu, Floquet-engineered diode performance of a topological Josephson junction composed of two Kitaev chains coupled via a quantum dot, Phys. Rev. B **112**, 125407 (2025).

[107] P.-M. Billangeon, F. Pierre, H. Bouchiat, and R. Deblock, Ac Josephson effect and resonant Cooper pair tunneling emission of a single Cooper pair transistor, Phys. Rev. Lett. **98**, 216802 (2007).

[108] J. Wiedenmann, E. Bocquillon, R. S. Deacon, S. Hartinger, O. Herrmann, T. M. Klapwijk, L. Maier, C. Ames, C. Brüne, C. Gould, A. Oiwa, K. Ishibashi, S. Tarucha, H. Buhmann, and L. W. Molenkamp, 4π-periodic Josephson supercurrent in HgTe-based topological Josephson junctions, Nat. Commun. **7**, 10303 (2016).

[109] S. Park, W. Lee, S. Jang, Y.-B. Choi, J. Park, W. Jung, K. Watanabe, T. Taniguchi, G. Y. Cho, and G.-H. Lee, Steady Floquet-Andreev states in graphene Josephson junctions, Nature (London) **603**, 421 (2022).